

GRAVITATIONAL WAVES FROM SUPERMASSIVE BLACK HOLE COALESCENCE IN A HIERARCHICAL GALAXY FORMATION MODEL

MOTOHIRO ENOKI¹, KAIKI T. INOUE^{1,2}, MASAHIRO NAGASHIMA^{3,4} AND NAOSHI SUGIYAMA¹

ABSTRACT

We investigate the expected gravitational wave emission from coalescing supermassive black hole (SMBH) binaries resulting from mergers of their host galaxies. When galaxies merge, the SMBHs in the host galaxies sink to the center of the new merged galaxy and form a binary system. We employ a semi-analytic model of galaxy and quasar formation based on the hierarchical clustering scenario to estimate the amplitude of the expected stochastic gravitational wave background owing to inspiraling SMBH binaries and bursts owing to the SMBH binary coalescence events. We find that the characteristic strain amplitude of the background radiation is $h_c(f) \sim 10^{-16}(f/1\mu\text{Hz})^{-2/3}$ for $f \lesssim 1\mu\text{Hz}$ just below the detection limit from measurements of the pulsar timing provided that SMBHs coalesce simultaneously when host galaxies merge. The main contribution to the total strain amplitude of the background radiation comes from SMBH coalescence events at $0 < z < 1$. We also find that a future space-based gravitational wave interferometer such as the planned *Laser Interferometer Space Antenna* (LISA) might detect intense gravitational wave bursts associated with coalescence of SMBH binaries with total mass $M_{\text{tot}} < 10^7 M_\odot$ at $z \gtrsim 2$ at a rate $\sim 1.0 \text{ yr}^{-1}$. Our model predicts that burst signals with a larger amplitude $h_{\text{burst}} \sim 10^{-15}$ correspond to coalescence events of massive SMBH binary with total mass $M_{\text{tot}} \sim 10^8 M_\odot$ at low redshift $z \lesssim 1$ at a rate $\sim 0.1 \text{ yr}^{-1}$ whereas those with a smaller amplitude $h_{\text{burst}} \sim 10^{-17}$ correspond to coalescence events of less massive SMBH binary with total mass $M_{\text{tot}} \sim 10^6 M_\odot$ at high redshift $z \gtrsim 3$.

Subject headings: black hole physics – galaxies:evolution – galaxies:formation – gravitational waves – quasars:general

1. INTRODUCTION

In recent years, there has been increasing observational evidence that many nearby galaxies have central supermassive black holes (SMBHs) in the mass range of $10^6 - 10^9 M_\odot$, and that their physical properties correlate with those of spheroids⁵ of their host galaxies. First, the estimated mass of a SMBH in a galactic center, M_{BH} , is roughly proportional to the mass of the spheroid, M_{spheroid} . The ratio of $M_{\text{BH}}/M_{\text{spheroid}}$ is $0.001 - 0.006$ in each galaxy (e.g. Kormendy & Richstone 1995; Magorrian et al. 1998; Merritt & Ferrarese 2001b). Second, the mass of a SMBH correlates with the velocity dispersion of stars in the spheroid, σ_{spheroid} , as $M_{\text{BH}} \propto \sigma_{\text{spheroid}}^n$, $n = 3.7 - 5.3$ (e.g. Ferrarese & Merritt 2000; Gebhardt et al. 2000; Merritt & Ferrarese 2001a; Tremaine et al. 2002). These relations suggest that the formation of SMBHs physically links to the formation of spheroids that harbor the SMBHs.

In order to study the formation and evolution of SMBHs, it is necessary to construct a model that includes galaxy formation and merger processes. It has become widely accepted that quasars are fueled by accretion of gas onto SMBHs in the nuclei of host galaxies. Hydrodynamical simulations have shown that a merger of galaxies drives gas fall rapidly onto the center of the merged system and fuels a nuclear starburst leading to spheroid formation (e.g. Mihos & Hernquist 1994, 1996; Barnes & Hernquist 1996). Some observations of quasar hosts show that many quasars reside in spheroids of interacting systems or elliptical galaxies (e.g. Bahcall et al. 1997; McLure et al. 1999; Dunlop et al. 2003; Kauffmann et al. 2003). Thus the major merger of galaxies is a possible mechanism for quasar activity, SMBH evolution and spheroid formation.

In the standard hierarchical structure formation scenario in a cold dark matter (CDM) universe, dark-matter halos (*dark halos*) cluster gravitationally and merge together. In each of merged dark halos, a galaxy is formed as a result of radiative gas cooling, star formation, and supernova feedback. Several galaxies in a common dark halo sometimes merge together and a more massive galaxy is assembled. When galaxies merge, SMBHs in the centers of the galaxies sink toward the center of the new merged galaxy and form a SMBH binary subsequently. If the binary loses enough energy and angular momentum, it will evolve to the gravitational wave emitting regime and begin inspiraling, eventually coalesces with a gravitational wave burst.

An ensemble of gravitational waves from a number of inspiraling SMBH binaries at different redshift can be observed

Electronic address: enoki.motohiro@nao.ac.jp

Electronic address: kinoue@phys.kindai.ac.jp

Electronic address: masa@scphys.kyoto-u.ac.jp

Electronic address: naoshi@th.nao.ac.jp

¹ National Astronomical Observatory, Osawa 2-21-1, Mitaka, Tokyo, 181-8588, Japan

² Present address: Department of Natural Science and Engineering, Kinki University, Higashi-Osaka, Osaka, 577-8502, Japan

³ Department of Physics, University of Durham, South Road, Durham DH1 3LE, U.K.

⁴ Present address: Department of Physics, Kyoto University, Sakyo-ku, Kyoto, 606-8502, Japan

⁵ Throughout this paper, we refer to bulge or elliptical galaxy as *spheroid*.

as a stochastic background at frequencies $\sim 1\text{ n} - 1\mu\text{Hz}$, which can be detected by pulsar timing measurements (Detweiler 1979). Gravitational wave bursts from coalescence events can be detected by a Doppler tracking test of interplanetary spacecraft (Thorne & Braginsky 1976). Future space interferometers such as the Laser Interferometer Space Antenna *LISA* might detect quasi-monochromatic wave sources associated with inspiraling SMBH binaries and gravitational wave bursts associated with SMBH binary coalescence.

In order to estimate the feasibility of detecting such gravitational waves, we need to know the SMBH coalescing rate that depends on the complex physical processes before coalescence. A possible scenario of forming SMBHs consists of four stages: First, a seed massive black hole in the center of a galaxy grows to an intermediate mass black hole (IMBH) via run-away collapse in a dense star cluster (Portegies Zwart, et al. 2004). Second, a galaxy that contains an IMBH in their center merges with another galaxy with an IMBH. Third, the two IMBHs sink to the center of gravitational potential well owing to dynamical friction until a “hardening” regime (Volonteri, Haardt & Madau 2003). Finally, physical processes such as three-body processes, gas dynamics, the “Kozai” mechanism, etc. drive the binary to the gravitational wave emission regime (e.g. Begelman, Blandford & Rees 1980; Makino 1997; Gould & Rix 2000; Yu 2002; Armitage & Natarajan 2002; Blaes, Lee, & Socrates 2002; Volonteri, Haardt & Madau 2003; Milosavljevic & Merritt 2003). However, the efficiency to bring two SMBHs together is still unknown.

To date, a number of attempts have been made to calculate the SMBH coalescence rate taking the physical processes in the “second” and “third” stages into account. Some authors use phenomenological models of galaxy mergers based on number counts of quasars and spheroids (e.g. Thorne & Braginsky 1976; Fukushima, Ebisuzaki & Makino 1992; Haehnelt 1994; Rajagopal & Romani 1995; Jaffe & Backer 2003). Others use merger rates of dark halos (not galaxies) based on formalism of Press & Schechter (1974) and Lacey & Cole (1993) (e.g. Haehnelt 1994; Menou, Haiman & Narayanan 2001). Volonteri, Haardt & Madau (2003) calculated the SMBH coalescence rate taking conditions under which “sub-halos” with SMBHs in a dark halo sink to the dark halo center into account (see also Wyithe & Loeb 2003; Sesana et al. 2004). However, none of these models include baryonic gas evolution and galaxy formation processes. Because SMBH formation process is relevant to spheroids of host galaxies rather than to dark halos, we need to evaluate how the baryonic gas processes such as star formation and radiative cooling affect the SMBH coalescence rate.

In this paper, we estimate the SMBH coalescence rate using a new semi-analytic (SA) model of Enoki et al. (2003) (an extended model of Nagashima et al. (2001)) in which the SMBH formation is incorporated into the galaxy formation. Then, we calculate the spectrum of gravitational wave background from inspiraling SMBH binaries, based on the formulation given by Jaffe & Backer (2003) and we compare our result with that from a pulsar timing measurement. We also estimate the event rate of gravitational wave bursts from SMBH coalescence events that might be detected by future planned space laser interferometers, based on an argument in Thorne & Braginsky (1976).

In SA models, merging histories of dark halos are realized using a Monte-Carlo algorithm and evolution of baryonic components within dark halos is calculated using simple analytic models for gas cooling, star formation, supernova feedback, galaxy merging and other processes. SA models have successfully reproduced a variety of observed features of galaxies, such as their luminosity functions, color distributions, and so on (e.g. Kauffmann et al. 1993; Cole et al. 1994, 2000; Somerville & Primack 1999; Nagashima et al. 2001, 2002). Kauffmann & Haehnelt (2000) introduced a unified model that includes the formation of both galaxies and SMBHs within the framework of their SA model (see also Cattaneo 2001; Menci et al. 2003; Islam, Taylor & Silk 2003; Granato et al. 2004). Our SA model reproduces not only these observational features but also the observed present black hole mass function and the quasar luminosity functions at different redshifts (Enoki et al. 2003).

The paper is organized as follows: in section 2 we briefly review our SA model for galaxy formation and SMBH growth; in section 3 we calculate the spectrum of gravitational wave background and the event rate of gravitational wave bursts; in section 4 we provide summary and conclusions.

2. GALAXY MERGER / BLACK HOLE COALESCENCE RATE

In this section we briefly describe our SA model for galaxy formation and the SMBH growth. The details are shown in Nagashima et al. (2001) and Enoki et al. (2003).

2.1. Model of Galaxy Formation

First, we construct Monte Carlo realizations of merging histories of dark halos from the present to higher redshifts using a method of Somerville & Kolatt (1999), which is based on the extended Press-Schechter formalism (Press & Schechter 1974; Bond et al. 1991; Bower 1991; Lacey & Cole 1993). Merging histories of dark halos depend on the cosmological model. The adopted cosmological model is a low-density, spatially flat cold dark matter (Λ CDM) universe with the present density parameter, $\Omega_m = 0.3$, the cosmological constant, $\Omega_\Lambda = 0.7$, the Hubble constant $h = 0.7$ ($h \equiv H_0/100 \text{ km s}^{-1} \text{ Mpc}^{-1}$) and the present rms density fluctuation in spheres of $8h^{-1}\text{Mpc}$ radius, $\sigma_8 = 0.9$. Dark halos with circular velocity, $V_{\text{circ}} < 40 \text{ km s}^{-1}$, are treated as diffuse accretion matter. This condition comes from the estimation of Jeans mass in the ultraviolet background radiation field (e.g. Thoul & Weinberg 1996). The adopted timestep of merging histories of dark halos is a redshift interval of $\Delta z = 0.06(1+z)$, corresponding to dynamical time scale of dark halos which collapse at redshift z . The highest redshift in each merging path which depends on the present dark halo mass, is about $z \sim 20 - 30$.

Next, in each merging path of dark halos, we calculate the evolution of the baryonic component from higher redshifts to the present. If a dark halo has no progenitor halos, the mass fraction of the gas in the halo is given by Ω_b/Ω_m where Ω_b is the baryonic density parameter. Here we use $\Omega_b = 0.02h^{-2}$. When a dark halo collapses, the gas in the

halo is shock-heated to the virial temperature of the halo (the *hot gas*). At the same time, the gas in dense regions of the halo cools owing to efficient radiative cooling and sinks to the center of the halo and settle into a rotationally supported disk until the subsequent collapse of the dark halo. We call this cooled gas the *cold gas*. Stars are formed from the cold gas at a rate of $\dot{M}_* = M_{\text{cold}}/\tau_*$, where M_{cold} is the mass of the cold gas and τ_* is the time scale of star formation. We assume $\tau_* = \tau_*^0 (V_{\text{circ}}/300 \text{ km s}^{-1})^{\alpha_*}$. The free parameters of τ_*^0 and α_* are chosen to match the observed mass fraction of cold gas in the disks of spiral galaxies. With star formation, supernovae occur and heat up the surrounding cold gas to the hot gas phase (supernova feedback). The reheating rate is given by $\dot{M}_{\text{reheat}} = \beta(V_{\text{circ}})\dot{M}_*$, where $\beta(V_{\text{circ}}) = (V_{\text{hot}}/V_{\text{circ}})^{\alpha_{\text{hot}}}$. The free parameters of V_{hot} and α_{hot} are determined by matching the observed local luminosity function of galaxies. Given the star formation rate as a function of time, we calculate the luminosity and color of each galaxy from the star formation history of the galaxy by using a stellar population synthesis model. We use the population synthesis code by Kodama & Arimoto (1997).

When several progenitor halos merge, a newly formed larger dark halo contains at least two or more galaxies which originally resided in the individual progenitor halos. We identify the central galaxy in the new common halo with the central galaxy contained in the most massive progenitor halos. Note that cooled hot gas accretes to only central galaxies. Other galaxies are regarded as satellite galaxies. These galaxies merge by either dynamical friction or random collision. Satellite galaxies merge with the central galaxy owing to dynamical friction in the following time scale,

$$\tau_{\text{fric}} = \frac{260}{\ln \Lambda_c} \left(\frac{R_H}{\text{Mpc}} \right)^2 \left(\frac{V_{\text{circ}}}{10^3 \text{ km s}^{-1}} \right) \left(\frac{M_{\text{sat}}}{10^{12} M_\odot} \right)^{-1} \text{ Gyr}, \quad (1)$$

where R_H and V_{circ} are the radius and the circular velocity of the new common halo, respectively, $\ln \Lambda_c$ is the Coulomb logarithm, and M_{sat} is the mass of the satellite galaxy including its dark halo (Binney & Tremaine 1987). When the time passing after a galaxy became a satellite exceeds τ_{fric} , the satellite galaxy infalls onto the central galaxy. On the other hand, satellite galaxies merge with each other in timescale of random collision. Under the condition that the satellite galaxies gravitationally bound and merge during encounters, the collision time scale is (Makino & Hut 1997),

$$\begin{aligned} \tau_{\text{coll}} = & \frac{500}{N^2} \left(\frac{R_H}{\text{Mpc}} \right)^3 \left(\frac{r_{\text{gal}}}{0.12 \text{ Mpc}} \right)^{-2} \\ & \times \left(\frac{\sigma_{\text{gal}}}{100 \text{ km s}^{-1}} \right)^{-4} \left(\frac{\sigma_{\text{halo}}}{300 \text{ km s}^{-1}} \right)^3 \text{ Gyr}, \end{aligned} \quad (2)$$

where N is the number of satellite galaxies, r_{gal} is a radius of a satellite, and σ_{halo} and σ_{gal} are the 1D velocity dispersions of the common halo and the satellite galaxy, respectively. With a probability of $\Delta t/\tau_{\text{coll}}$, where Δt is the timestep corresponding to the redshift interval Δz , a satellite galaxy merges with another randomly picked satellite. Let us consider the case that two galaxies of masses m_1 and $m_2 (> m_1)$ merge together. If the mass ratio, $f = m_1/m_2$, is larger than a certain critical value of f_{bulge} (major merger), we assume that a starburst occurs: all of the cold gas turns into stars and hot gas which fills the dark halo, and all of the stars populate the bulge of a new galaxy. On the other hand, if $f < f_{\text{bulge}}$ (minor merger), no starburst occurs and a smaller galaxy is simply absorbed into the disk of a larger galaxy. These processes are repeated until the output redshift. We classify galaxies into different morphological types according to the B -band bulge-to-disk luminosity ratio, B/D . In this paper, galaxies with $B/D > 2/3$, and $B/D \leq 2/3$ are classified as ellipticals/S0s and spirals, respectively. The parameter f_{bulge} is fixed by a comparison with the observed type mix.

Model parameters are determined by a comparison with observations of galaxies in the local Universe, such as luminosity functions and the cold gas mass fraction in spiral galaxies. Our SA model can reproduce galaxy number counts and photometric redshift distribution of galaxies in the Hubble Deep Field. The adopted parameters of this model are tabulated in table 1. Some of the model parameters (σ_8 , Ω_b and fraction of invisible stellar mass Υ) are updated and slightly different from our previous paper (Nagashima et al. 2001; Enoki et al. 2003). The update of σ_8 and Ω_b causes only a slight change of Υ and we have confirmed that the modification hardly affects our results. Using this SA model, we can estimate the galaxy merger rate at each redshift.

2.2. The growth of SMBH

Let us briefly summarize the growth model of SMBHs introduced by Enoki et al. (2003). In this model, it is assumed that SMBHs grow by coalescence when their host galaxies merge and are fueled by accreted cold gas during major mergers of galaxies. When the host galaxies merge, pre-existing SMBHs sink to the center of the new merged galaxy due to dynamical friction (or other mechanisms such as gas dynamics), evolve to the gravitational wave emission regime and eventually coalesce. Although the timescale for this process is unknown, for the sake of simplicity we assume that SMBHs instantaneously evolve to the gravitational wave emission regime and coalesce. Gas-dynamical simulations have demonstrated that the major merger of galaxies can drive substantial gaseous inflows and trigger starburst activity (e.g. Mihos & Hernquist 1994, 1996; Barnes & Hernquist 1996). Thus, it is reasonable to assume that during a major merger of galaxies, a certain fraction of the cold gas that is proportional to the total mass of stars newly formed at starburst accretes onto the newly formed SMBH and this accretion process leads to a quasar activity. Under this assumption, the mass of cold gas accreted on a SMBH is given by

$$M_{\text{acc}} = f_{\text{BH}} \Delta M_{*, \text{burst}}, \quad (3)$$

where f_{BH} is a constant and $\Delta M_{*,\text{burst}}$ is the total mass of stars formed at starburst. The free parameter of f_{BH} is fixed by matching the observed relation between a spheroid mass and a black hole mass $M_{\text{BH}}/M_{\text{spheroid}} = 0.001 - 0.006$ (e.g. Magorrian et al. 1998); we find that the favorable value of f_{BH} is nearly 0.03.

Figure 1 shows the model prediction of the growth rate of the averaged SMBH mass, $\langle \dot{M}_{\text{BH}} \rangle$. We define the averaged SMBH mass growth rate as follows,

$$\langle \dot{M}_{\text{BH}} \rangle = \frac{\int \dot{M}_{\text{BH}} \phi_{\text{BH}}(M_{\text{BH}}, z) dM_{\text{BH}}}{\int \phi_{\text{BH}}(M_{\text{BH}}, z) dM_{\text{BH}}}, \quad (4)$$

where \dot{M}_{BH} is the mass increase rate of SMBH with M_{BH} at z , and $\phi_{\text{BH}}(M_{\text{BH}}, z)$ is the black hole mass function. \dot{M}_{BH} is given by $\dot{M}_{\text{BH}} = (M_{\text{acc}} + M_{\text{coal}})/\Delta t$ where M_{coal} is the mass increment due to SMBH binaries coalescence (the mass of smaller SMBH). This figure shows the SMBH mass growth is mostly due to gas accretion and does not depend on initial seed masses. At lower redshift ($z \lesssim 1$), since the cold gas is depleted by star formation, the SMBH coalescence becomes a dominant process of the SMBH mass growth.

Figure 2 (a) shows the black hole mass functions in our model at a series of various redshifts. This indicates that the number density of the most massive black holes increases monotonically with time in our scenario in which SMBHs grow by an accretion of cold gas and by coalescence. In this figure, we superpose the black hole mass function at $z = 0$ obtained by Salucci et al. (1999). The present mass function in our model is quite consistent with the observation. Our galaxy formation model includes dynamical friction and random collision as galaxy merging mechanisms. For comparison, in figure 2 (b), we also plot the black hole mass functions at $z = 0$ of other two models: no random collision model (no rc model) and no dynamical friction model (no df model). In the no rc model and the no df model, mergers owing to random collision and dynamical friction are switched off, respectively. This figure shows that the mass function for low mass black holes are determined by random collisions between satellite galaxies and that for high mass black holes are influenced by dynamical friction. The shape of black hole mass function depends on detailed gas processes. The important contribution of mass increment of SMBHs in central galaxies is the cold gas, which is accreted to only central galaxies. SNe feedback removes this cold gas more efficiently in smaller galaxies with $V_{\text{circ}} < V_{\text{hot}} = 280 \text{ km s}^{-1}$ ($M_{\text{gal}} < 10^{12} M_{\odot}$). Thus, the growth of the SMBHs in small central galaxies suffers from SNe feedback. In the no rc model, SMBHs mainly exist central galaxies. Therefore, the shape of the black hole mass function in the no rc model has a bump at high mass end ($M_{\text{BH}} \sim 10^9 M_{\odot}$) which corresponds to SMBHs in the central galaxies ($M_{\text{gal}} \sim 10^{12} M_{\odot}$). On the other hand, in the no df model, high mass SMBHs cannot be produced since galaxies cannot merge with the massive central galaxy.

Enoki et al. (2003) investigated environments and clustering properties of quasars using this SA model which can also reproduce quasar luminosity functions at different redshifts. While our approach is similar to Kauffmann & Haehnelt (2000), their star formation and feedback models are different from ours and their model does not include the random collision process. Therefore, their resultant model description differs from ours in equation (3). Using the SA model incorporated with this SMBH growth model, we estimate the comoving number density, $n_c(M_1, M_2, z) dM_1 dM_2 dz$, of the coalescing SMBH binaries with mass $M_1 \sim M_1 + dM_1$ and $M_2 \sim M_2 + dM_2$ at z in a given redshift interval dz .

It is difficult to know how SMBH binaries manage to shrink to a gravitational wave emission regime after their host galaxies merge, because all physical processes and conditions related to this problem are still not clear (dynamical friction, stellar distribution, triplet SMBH interaction, gas dynamical effects and so on). Nevertheless, many authors have tackled this problem (e.g. Begelman, Blandford & Rees 1980; Makino 1997; Gould & Rix 2000; Yu 2002; Armitage & Natarajan 2002; Blaes, Lee, & Socrates 2002; Milosavljevic & Merritt 2003). In what follows, we assume that SMBHs coalesce simultaneously when host galaxies merge for simplicity. In other words, the efficiency of SMBH coalescence is assumed to be maximum. Note that Volonteri, Haardt & Madau (2003) constructed a SMBH growth model in which the merging history of dark halos with SMBHs in their center is derived from cosmological Monte-Carlo simulations. Although they incorporated dynamical evolution of SMBH binaries and triplet SMBH interactions into their model, no galaxy formation process is taken into account.

3. GRAVITATIONAL RADIATION

3.1. Background radiation from SMBH binaries

In order to calculate the spectrum of gravitational wave background radiation from SMBH binaries, it is necessary to follow the orbit evolution of each binary. However, it is difficult to set initial conditions. To avoid this problem, we adopt a formulation by Jaffe & Backer (2003) (see also Rajagopal & Romani 1995).

We start calculation of the expected amplitude of gravitational radiation emitted by a binary. We assume that a binary orbit is circular for simplicity⁶. The amplitude is given by (Thorne 1987)

$$\begin{aligned} h_s(z, f, M_1, M_2) &= 4 \sqrt{\frac{2}{5}} \frac{(GM_{\text{chirp}})^{5/3}}{c^4 D(z)} (2\pi f_p)^{2/3} \\ &= 3.5 \times 10^{-17} \left(\frac{M_{\text{chirp}}}{10^8 M_{\odot}} \right)^{5/3} \left[\frac{D(z)}{1 \text{ Gpc}} \right]^{-1} \left[\frac{f(1+z)}{10^{-7} \text{ Hz}} \right]^{2/3}, \end{aligned} \quad (5)$$

⁶ Note that the initial orbit of a binary is not necessarily circular. Since the amplitude and timescale of gravitational wave emissions are sensitive to eccentricity of a binary orbit (Peters & Matthews 1963), the initial distribution of eccentricity affects the final expected amplitudes. However, we assume that the orbit becomes circular immediately.

where $M_{\text{chirp}} = [M_1 M_2 (M_1 + M_2)^{-1/3}]^{3/5}$ is the chirp mass of the system and c is the speed of light. f_p is the reciprocal of the proper rest-frame period of the binary, which is related to the observed frequency, f , of the gravitational wave from the binary in a circular orbit as $f = 2f_p/(1+z)$. $D(z)$ is the comoving distance to the binary

$$D(z) = \frac{c}{H_0} \int_0^z \frac{dz'}{\sqrt{\Omega_m(1+z')^3 + \Omega_\Lambda}}. \quad (6)$$

Next, we calculate $\nu(M_1, M_2, z) dM_1 dM_2 dz$, the number of coalescing SMBH binaries with mass M_1 and M_2 in mass intervals dM_1 and dM_2 per observers' time occurring at z in a given redshift interval dz ,

$$\begin{aligned} \nu(M_1, M_2, z) &= \frac{dV}{dt_0} n_c(M_1, M_2, z) \\ &= \frac{1}{(1+z)} \frac{dV}{dt_p} n_c(M_1, M_2, z), \end{aligned} \quad (7)$$

where t_0 is the observers' time, t_p is the proper rest-frame time at z and dV is the comoving volume element at $z \sim z + dz$ given by

$$\frac{dV}{dt_p} = 4\pi(1+z)cD(z)^2. \quad (8)$$

The timescale emitting gravitational waves of a binary measured in the rest-frame is

$$\tau_{\text{GW}} \equiv f_p \frac{dt_p}{df_p}. \quad (9)$$

Since the timescale in the observer-frame is $\tau_{\text{GW,obs}} = \tau_{\text{GW}}(1+z)$, for a binary in a circular orbit at redshift z , it is expressed as (Peters & Matthews 1963)

$$\begin{aligned} \tau_{\text{GW,obs}}(M_1, M_2, z, f) &= \frac{5}{96} \left(\frac{c^3}{GM_{\text{chirp}}} \right)^{5/3} [2\pi f_p]^{-8/3} (1+z) \\ &= 1.2 \times 10^4 \left(\frac{M_{\text{chirp}}}{10^8 M_\odot} \right)^{-5/3} \left[\frac{f}{10^{-7} \text{ Hz}} \right]^{-8/3} (1+z)^{-5/3} \text{ yr}. \end{aligned} \quad (10)$$

As a SMBH binary evolves with time, the frequency becomes higher. We assume that the binary orbit is quasi-stationary (i.e. phase evolution time scale is less than τ_{GW}) until the radius equals to $3R_s$, where R_s is the Schwarzschild radius : the radius of the innermost stable circular orbit (ISCO) for a particle and a non-rotating black hole. Then the maximum frequency f_{max} is

$$\begin{aligned} f_{\text{max}}(M_1, M_2, z) &= \frac{c^3}{6^{3/2} \pi G M_1 (1+z)} \left(1 + \frac{M_2}{M_1} \right)^{1/2} \\ &= 4.4 \times 10^{-5} (1+z)^{-1} \left(\frac{M_1}{10^8 M_\odot} \right)^{-1} \left(1 + \frac{M_2}{M_1} \right)^{1/2} \text{ Hz}, \end{aligned} \quad (11)$$

where M_1 and M_2 are SMBH masses ($M_1 > M_2$). The number of coalescing SMBH binaries as a source of gravitational wave source with observed frequency f at redshift z is estimated as

$$\nu(M_1, M_2, z) dz dM_1 dM_2 \tau_{\text{GW,obs}} \theta(f_{\text{max}} - f), \quad (12)$$

where $\theta(x)$ is the step function. Therefore, from equations (5), (7), (10) and (13), we finally obtain the spectrum of the gravitational wave background radiation,

$$\begin{aligned} h_c^2(f) &= \int dz dM_1 dM_2 h_s^2 \nu(M_1, M_2, z) \tau_{\text{GW,obs}} \theta(f_{\text{max}} - f). \\ &= \int dz dM_1 dM_2 \frac{4\pi c^3}{3} \left(\frac{GM_{\text{chirp}}}{c^3} \right)^{5/3} (\pi f)^{-4/3} (1+z)^{-1/3} n_c(M_1, M_2, z) \theta(f_{\text{max}} - f). \end{aligned} \quad (13)$$

We note that the equation (13) agrees with the result of Phinney (2001) except for the step function, $\theta(f_{\text{max}} - f)$. The original formulation of Jaffe & Backer (2003) does not include this effect, either.

As shown in figure 3, the spectrum changes its slope at $f \sim 1\mu\text{Hz}$ owing to lack of power associated with the upper limit frequency, f_{max} . This feature is consistent with the results of Wyithe & Loeb (2003) and Sesana et al. (2004). The predicted strain spectrum is $h_c(f) \sim 10^{-16} (f/1\mu\text{Hz})^{-2/3}$ for $f \lesssim 1\mu\text{Hz}$, just below the current limit from the pulsar timing measurements by Lommen (2002). In our model, we assume that SMBHs coalesce simultaneously when their host galaxies merge. Therefore, the efficiency of SMBH coalescence is maximum and the predicted amplitude of gravitational wave spectrum should be interpreted as the upper limit.

In figure 3 (a), we plot the spectra from binaries in different redshift intervals. This figure shows that the total spectrum of background radiation comes from coalescing SMBH binaries at low redshift, $0 \leq z < 1$. In figure 4, we plot the SMBH coalescence rate in observers' time unit a year, $\nu(z) = \int \nu(M_1, M_2, z) dM_1 dM_2$. This figure indicates that the coalescence rate at low redshift is lower than the coalescence rate at high redshift. However, the main contribution to the background radiation is gravitational wave from the coalescing SMBH binaries at low redshift, $0 \leq z < 1$, because the distance from an observer to the SMBH binaries at low redshift is shorter and the mass of SMBHs at low redshift is higher. In figure 3(b), we also plot the spectra from binaries in different total mass intervals ($M_{\text{tot}} = M_1 + M_2$). This figure shows that for $f \gtrsim 10^{-4}\text{Hz}$ the total spectrum of background radiation comes from coalescing SMBH binaries with total mass $M_{\text{tot}} \lesssim 10^8 M_\odot$.

When SMBHs are spinning and/or when their masses are comparable, the definition of ISCO becomes vague and our assumption that the cutoff frequency f_{max} corresponds to $3R_S$ may not be correct. To see the effects of the cutoff frequency, we plot the spectra for different values of f_{max} , corresponding to $3R_S$, $30R_S$, and no frequency cut off, respectively (figure 5 (a)). Lowering f_{max} causes a suppression in the stochastic background at high frequencies $f \lesssim 10^{-7}\text{Hz}$ since a large portion of high frequency modes are cut off. As shown in this figure, the cut off radius does not affect the amplitude at the frequency of the pulsar timing measurement $f \simeq 10^{-9}\text{Hz}$.

Our galaxy formation model incorporates dynamical friction and random collision as galaxy merging mechanisms. In order to examine the effect of these two galaxy merger mechanisms on the spectrum of gravitational wave background radiation, in figure 5 (b), we also plot the spectrum of background radiation of other two models: no rc model and no df model. The no df model can not produce higher mass SMBH (see fig. 2(b)). Consequently, the spectrum in no df model bends at larger frequency since the number of SMBHs with smaller f_{max} decreases. Furthermore, in the no df model, the amplitude of gravitational waves from each binary becomes smaller. However, the coalescence rate in no df model is higher than the rate in no rc model as shown in figure 4. As a result, the amplitude of the spectrum in no df model is roughly equal to the amplitude in no rc model.

3.2. Gravitational wave burst from SMBH coalescence

After an inspiraling phase, SMBHs plunge into a final death inspiral and merge to form a single black hole. We call a set of a plunge and a subsequent early non-linear ring-down phase as a *burst*⁷. In this subsection, we estimate the expected burst event rate per observers' time using the amplitude of burst gravitational wave given by Thorne & Braginsky (1976), and the SMBH coalescence rate calculated by our SA model, $n_c(M_1, M_2, z)$.

The gravitational wave amplitude is given by

$$h^2 = \frac{2GF_{\text{GW}}}{\pi c^3 f_c^2}, \quad (14)$$

where F_{GW} is the energy flux of the gravitational wave at the observer and f_c is the observed characteristic frequency. f_c from the gravitational wave burst occurring at z is

$$\begin{aligned} f_c &= \frac{c^3}{3^{3/2} G M_{\text{tot}} (1+z)} \\ &= 3.9 \times 10^{-4} \left(\frac{M_{\text{tot}}}{10^8 M_\odot} \right)^{-1} (1+z)^{-1} \text{Hz}, \end{aligned} \quad (15)$$

where M_{tot} is total mass of the black holes. The energy flux from the burst gravitational wave occurring at z is given by

$$F_{\text{GW}} = \frac{\epsilon M_{\text{tot}} c^2 f_c}{4\pi D(z)^2 (1+z)}, \quad (16)$$

where ϵ is the efficiency of the energy release and $D(z)$ is the distance to the source from the observer given by equation (6). From equations (14), (15) and (16), the characteristic amplitude of the burst gravitational wave is

$$\begin{aligned} h_{\text{burst}} &= \frac{3^{3/4} \epsilon^{1/2} G M_{\text{tot}}}{2^{1/2} \pi c^2 D(z)} \\ &= 7.8 \times 10^{-16} \left(\frac{\epsilon}{0.1} \right)^{1/2} \left(\frac{M_{\text{tot}}}{10^8 M_\odot} \right) \left[\frac{D(z)}{1 \text{ Gpc}} \right]^{-1}. \end{aligned} \quad (17)$$

Equations (15) and (17) show that we can estimate the amplitude and the characteristic frequency of the burst gravitational wave, once we know the total mass and redshift of coalescing SMBHs. From eq.(15), eq.(17) and $n_c(M_1, M_2, z)$, we obtain $n_{\text{burst}}(h_{\text{burst}}, f_c, z) dh_{\text{burst}} df_c dz$, which is the comoving number density of gravitational wave burst events occurring at z in a given redshift interval dz with amplitude $h_{\text{burst}} \sim h_{\text{burst}} + dh_{\text{burst}}$ and with characteristic frequency $f_c \sim f_c + df_c$. Then, the expected event rates of gravitational wave bursts per observers' time

⁷ Later ring-down phase at linear perturbation regime is not included.

with amplitude $h_{\text{burst}} \sim h_{\text{burst}} + dh_{\text{burst}}$ and characteristic frequency $f_c \sim f_c + df_c$, $\nu_{\text{burst}}(h_{\text{burst}}, f_c) dh_{\text{burst}} df_c$ is given by

$$\nu_{\text{burst}}(h_{\text{burst}}, f_c) = \int n_{\text{burst}}(h_{\text{burst}}, f_c, z) \frac{dV}{dt_0} dz. \quad (18)$$

The integrated event rates of gravitational wave bursts per observers' time with amplitude $h_{\text{burst}} \sim h_{\text{burst}} + dh_{\text{burst}}$, $\nu_{\text{burst}}(h_{\text{burst}}) dh_{\text{burst}}$, are given respectively as follows,

$$\nu_{\text{burst}}(h_{\text{burst}}) = \int \nu_{\text{burst}}(h_{\text{burst}}, f_c) df_c. \quad (19)$$

In figure 6, we plot the total integrated event rates of gravitational wave bursts and integrated event rates in different redshift intervals (figure 6(a)) and in different total mass intervals in (figure 6(b)). Here we set the efficiency of the energy release $\epsilon = 0.1$, while the precise value of this parameter is unknown. Flanagan & Hughes (1998) argued that the efficiency could reach 10 %, which depends on alignments of spin and parameter choices. In most typical events, a conversion efficiency will probably be a few percent (Baker et al. 2001). From equation (17), one can see that the change of efficiency results in the parallel displacement in the horizontal direction in figure 6. The shape of $\nu_{\text{burst}}(h_{\text{burst}})$ reflects the black hole mass functions and the SMBH coalescence rates, which depend on the complex galaxy formation processes. In figure 6 (a), one can notice that there are two peaks in the event rate in terms of h_{burst} . A peak at $h_{\text{burst}} \sim 10^{-17}$ corresponds to bursts from SMBH binaries with $M_{\text{tot}} < 10^6 M_\odot$ whose total number is the largest at high redshift $z > 3$. Another peak at $h_{\text{burst}} \sim 10^{-15}$ corresponds to bursts from SMBH binaries with $10^7 M_\odot < M_{\text{tot}} < 10^8 M_\odot$ whose coalescence probability is the largest at high redshift $z > 3$. Figure 6 (b) indicates that burst signals with large amplitude ($h_{\text{burst}} \gtrsim 10^{-15}$) correspond to coalescence of “massive” SMBH binaries with $M_{\text{tot}} \gtrsim 10^8 M_\odot$ occurring at $z \lesssim 1$. This is because the distance from the earth to SMBHs at low redshift is shorter and the mass of SMBHs at low redshift is larger. On the other hand, burst signals with amplitude ($h_{\text{burst}} \gtrsim 10^{-15}$) corresponds to coalescence events of “less massive” SMBH binaries with $M_{\text{tot}} \lesssim 10^7 M_\odot$ occurring at $z \gtrsim 2$. These events dominate the expected burst event rate provided that the sensitivity of the detector is sufficiently good. This feature is quite important because it breaks the degeneracy between mass and distance. Our model predicts that the expected rates of the coalescence events owing to SMBH binaries with small mass $M_{\text{tot}} < 10^6 M_\odot$ at low redshift and those with large mass $M_{\text{tot}} > 10^8 M_\odot$ at high redshift $z > 3$ are small.

Figure 7 shows that the expected region for signal of gravitational wave bursts and the instrumental noise threshold for *LISA*, h_{inst} . For randomly oriented sources, a sensitivity for a search of gravitational wave bursts in an observation time T_{obs} is given by (Thorne 1987; Haehnelt 1994)

$$h_{\text{inst}}^2 \sim \left(\frac{T_{\text{obs}}}{1 \text{ yr}} \right)^{-1} 10 S_h f_c, \quad (20)$$

where S_h is the spectral instrumental noise density. We compute h_{inst} from the fitting formula for S_h of *LISA* (Hughes 2002). The expected region for $\nu_{\text{burst}}[\log(h_{\text{burst}}), \log(f_c)] > 1 \text{ yr}^{-1}$ is above this instrumental noise threshold. For comparison, we show the region for $\nu_{\text{burst}}[\log(h_{\text{burst}}), \log(f_c)] > 1/5 \text{ yr}^{-1}$ and $\nu_{\text{burst}}[\log(h_{\text{burst}}), \log(f_c)] > 3 \text{ yr}^{-1}$ in figure 7 (b).

From figure 6 and 7, we conclude that the *LISA* can detect intense bursts of gravitational waves at a rate of $\sim 1.0 \text{ yr}^{-1}$ assuming that dominant part of these burst events occur at $z \gtrsim 2$. Even in the case of $\epsilon = 0.001$, the *LISA* can detect intense bursts of gravitational waves in one year observation, since $h_{\text{burst}} \propto \epsilon^{1/2}$. In addition, we find that large amplitude $h_{\text{burst}} \sim 10^{-15}$ signals correspond to coalescence events of massive SMBH binaries $M_{\text{tot}} \sim 10^8 M_\odot$ at low redshift $z \lesssim 1$ and small amplitude $h_{\text{burst}} \sim 10^{-17}$ signals correspond to less massive SMBH binaries $M_{\text{tot}} \sim 10^6 M_\odot$ at high redshift $z \gtrsim 3$.

Based on a SA-model (Kauffmann & Haehnelt 2000), Haehnelt (2003) concluded that *LISA* might detect SMBH coalescence events at a rate $0.1 \sim 1.0 \text{ yr}^{-1}$ over the redshift range of $0 \leq z \leq 5$ although no explicit calculation on gravitational wave emission is done. Our result is consistent with his result.

4. SUMMARY AND CONCLUSIONS

In this paper, we have estimated the coalescence rate of supermassive black hole (SMBH) binaries in the centers of galaxies using a new semi-analytic model of galaxy and quasar formation (SA model) given by Enoki et al. (2003) based on the hierarchical structure formation scenario. Then, we calculated the spectrum of the gravitational wave background from inspiraling SMBH binaries based on the formulation given by Jaffe & Backer (2003) and estimated the expected amplitudes and event rates of intense bursts of gravitational waves from coalescing SMBH binaries.

Our SA model includes dynamical friction and random collision as galaxy merging mechanisms, and assumes that a SMBH is fueled by accretion of cold gas during a major merger of galaxies leading to a spheroid formation, and that SMBHs coalesce simultaneously when host galaxies merge. Many previous other studies have paid attention to only SMBH growth and did not take galaxy formation processes into account. For investigating the relations between SMBH growth and galaxy formation processes, SA methods of galaxy and SMBH formation are suitable tools (Kauffmann & Haehnelt 2000; Cattaneo 2001; Enoki et al. 2003; Menci et al. 2003; Granato et al. 2004). Our SA model can reproduce not only observational properties of galaxies, but also the present SMBH mass function and the quasar luminosity functions at different redshifts (Nagashima et al. 2001; Enoki et al. 2003).

We have found that the gravitational wave background radiation spectrum for $f \lesssim 1\mu\text{Hz}$ has a characteristic strain $h_c(f) \sim 10^{-16}(f/1\mu\text{Hz})^{-2/3}$ just below the detection limit from the current measurements of the pulsar timing. The slope of the spectrum for $f \gtrsim 1\mu\text{Hz}$ gets steep owing to the upper limit in frequency set by the radius of the innermost stable circular orbit. The stochastic background radiation mainly comes from inspiraling SMBH binaries at $0 < z < 1$. Therefore, the background radiation can probe inspiraling SMBH binaries at low redshift.

We have also found that *LISA* might detect intense bursts of gravitational waves owing to the SMBH coalescence events at a rate $0.1 \sim 1.0 \text{ yr}^{-1}$ and that the main contribution to the event rate comes from SMBH binary coalescence at high redshift $z \gtrsim 2$. Our model predicts that burst signals with a large amplitude correspond to coalescence of large mass SMBH binaries at low redshift while those with a small amplitude correspond to coalescence of small mass SMBH binaries at high redshift. This prediction can be tested by future measurements of the amplitude and the phase evolution in gravitational waves from inspiraling SMBH binaries (Hughes 2002). Comparing these predictions with observations in future, we can put a stringent constraint on SMBH formation and evolution models.

We thank N. Gouda, K. Okoshi, S. Yoshioka and H. Yahagi for useful comments and discussions. We also thank K.S. Thorne and S. Hughes for useful information. MN acknowledges Research Fellowships of the Japan Society for the Promotion of Science for Young Scientists (No.00207) and support from the PPARC rolling grant for extragalactic astronomy and cosmology at Durham. NS is supported by Japanese Grant-in-Aid for Science Research Fund of the Ministry of Education, No.14340290. Numerical computations in this work were partly carried out at the Astronomical Data Analysis Center of the National Astronomical Observatory Japan.

REFERENCES

- Armitage, P. J. & Natarajan, P. 2002, *ApJ*, 567, L9
Bahcall, J. N., Kirhakos, S., Saxe, D. H., & Schneider, D. P. 1997, *ApJ*, 479, 642
Baker, J., Bruggmann, B., Campanelli, M., Lousto, O. & Takahashi, R. 2001, *Phys. Rev. Lett.*, 87, 121103
Barnes, J. E., & Hernquist, L. 1996, *ApJ*, 471, 115
Begelman, M. C., Blandford, R. D., & Rees, M. J. 1980, *Nature*, 287, 307
Binney, J., & Tremaine, S. 1987, *Galactic Dynamics*, Princeton, NJ, Princeton Univ. Press
Blaes, O., Lee, M. H., & Socrates, A. 2002, *ApJ*, 578, 775
Bond, J. R., Cole, S., Efstathiou, G., & Kaiser, N. 1991, *ApJ*, 379, 440
Bower, R. J. 1991, *MNRAS*, 248, 332
Cattaneo, A. 2001, *MNRAS*, 324, 128
Cole, S., Aragon-Salamanca, A., Frenk, C. S., Navarro, J. F., & Zepf, S. E. 1994, *MNRAS*, 271, 781
Cole, S., Lacey, C. G., Baugh, C. M., & Frenk, C. S. 2000, *MNRAS*, 319, 168
Detweiler, S. 1979, *ApJ*, 234, 1100
Dunlop, J. S. et al., 2003, *MNRAS*, 340, 1950
Enoki, M., Nagashima, M. & Gouda, N., 2003, *PASJ*, 55, 133
Ferrarese, L. & Merritt, D., 2000, *ApJ*, 539, L9
Flanagan, E. E., & Hughes, S. A. 1998, *Phys. Rev. D*, 57, 4535
Fukushige, T., Ebisuzaki, T. & Makino, J., 1992, *ApJ*, 396, L61
Gebhardt, K., Bender, R., Bower, G., Dressler, A., Faber, S. M., Filippenko, A. V., Green, R., Grillmair, C., et al., 2000, *ApJ*, 539, L13
Gould, A. & Rix, H. 2000, *ApJ*, 532, L29
Granato, G. L., De Zottie, G., Silva, L., Bressan, A., & Danese, L., 2004, *ApJ*, 600, 580
Haehnelt, M. G., 1994, *MNRAS*, 269, 199
Haehnelt, M. G., 2003, *Class. Quantum Grav.*, 20, S31
Hughes, S. A. 2002, *MNRAS*, 331, 805
Islam, R. R., Taylor, J. E. & Silk, J., 2003, *astro-ph/0309559*
Jaffe, A. H. & Backer, D. C., 2003, *ApJ*, 583, 616
Kauffmann, G., White, S. D. M., & Guiderdoni, 1993, *MNRAS*, 264, 201
Kauffmann, G., & Haehnelt, M. G. 2000, *MNRAS*, 311, 576
Kauffmann, G., et al., 2003, *MNRAS*, 346, 1055
Kodama, T., & Arimoto, N. 1997, *A&A*, 320, 41
Kormendy, J., & Richstone, D., 1995, *ARA&A*, 33, 581
Lacey, C. G., & Cole, S. 1993, *MNRAS*, 262, 627
Lommen, A. N. 2002, in the *Proceedings of the 270. WE-Heraeus Seminar on Neutron Stars, Pulsars and Supernova Remnants*, 2002, Physikzentrum Bad Honnef, eds. W. Becker, H. Lesch & J. Truemper.
Magorrian, J., et al., 1998, *AJ*, 115, 2285
Makino, J. 1997, *ApJ*, 478, 58
Makino, J., & Hut, P. 1997, *ApJ*, 481, 83
McLure, R. J., Kukula, M. J., Dunlop, J. S., Baum, S. A., O'Dea, C. P., & Hughes, D. H. 1999, *MNRAS*, 308, 377
Menci N., Cavaliere A., Fontana A., Giallongo E., Poli F., & Vittorini V., 2003, *ApJ*, 587, L63
Menou, K., Haiman, Z., & Narayanan, V. K. 2001, *ApJ*, 558, 535
Merritt, D., & Ferrarese, L. 2001, *ApJ*, 547, 140
Merritt, D., & Ferrarese, L. 2001, *MNRAS*, 320, L30
Mihos, J. C., & Hernquist, L. 1994, *ApJ*, 431, L9
Mihos, J. C., & Hernquist, L. 1996, *ApJ*, 464, 641
Milosavljevic, M. & Merritt, D., 2003, *ApJ*, 596, 860
Nagashima, M., Totani, T., Gouda, N., & Yoshii, Y. 2001, *ApJ*, 557, 505
Nagashima, M., Yoshii, Y., Totani, T., & Gouda, N. 2002, *ApJ*, 578, 675
Peters, P. & Matthews, J. 1963, *Phys. Rev.*, 13, 435
Phinney, E. S., 2001, *astro-ph/0108028*
Portegies Zwart, S. F., Baumgardt, H., Hut, P. & Makino, J. 2004, *Nature*, 428, 724
Press, W. H., & Schechter, P. 1974, *ApJ*, 187, 425
Rajagopal, M. & Romani, R., 1995, *ApJ*, 446, 543
Salucci, P., Szuszkiewicz, E., Monaco, P., & Danese, L. 1999, *MNRAS*, 307, 637
Sesana, A., Haardt, F., Madau, P., & Volonteri, M. 2004, *astro-ph/0401543*
Somerville, R. S., & Kolatt, T. S. 1999, *MNRAS*, 305, 1
Somerville, R. S., & Primack, J. R. 1999, *MNRAS*, 310, 1087
Thoul, A. A., & Weinberg, D. H. 1996, *ApJ*, 465, 608
Thorne, K. S. & Braginsky, V. B., 1976, *ApJ*, 204, L1
Thorne, K. S. 1987, in *Three Hundred Years of Gravitation*, ed. S. W. Hawking & W. Israel (Cambridge: Cambridge University Press)
Tremaine, S. et al., 2002, *ApJ*, 574, 740
Volonteri, M., Haardt, F. & Madau, P., 2003 *ApJ*, 582, 559
Wyithe, J. S. B., & Loeb, A. 2003, *ApJ*, 590, 691
Yu, Q. 2002, *MNRAS*, 331, 935

TABLE 1
MODEL PARAMETERS.

Cosmological parameters					Astrophysical parameters						
Ω_m	Ω_Λ	h	σ_8	Ω_b	$V_{\text{hot}} \text{ (km s}^{-1}\text{)}$	α_{hot}	$\tau_*^0 \text{ (Gyr)}$	α_*	f_{bulge}	Υ	
0.3	0.7	0.7	0.9	$0.02h^{-2}$	280	2.5	1.5	-2	0.5	1.7	

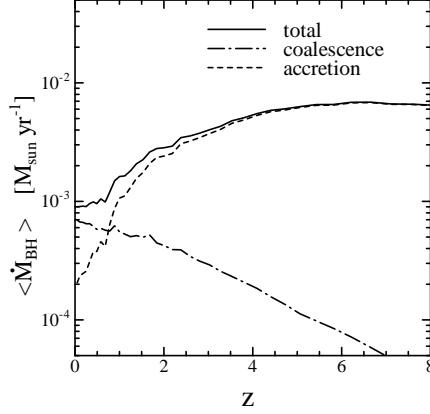


FIG. 1.— Averaged SMBH mass growth rate, $\langle \dot{M}_{\text{BH}} \rangle$, of the model. The solid, dot-dashed and short dashed lines indicate SMBH mass growth rate of total, due to SMBH coalescence and due to gas accretion, respectively.

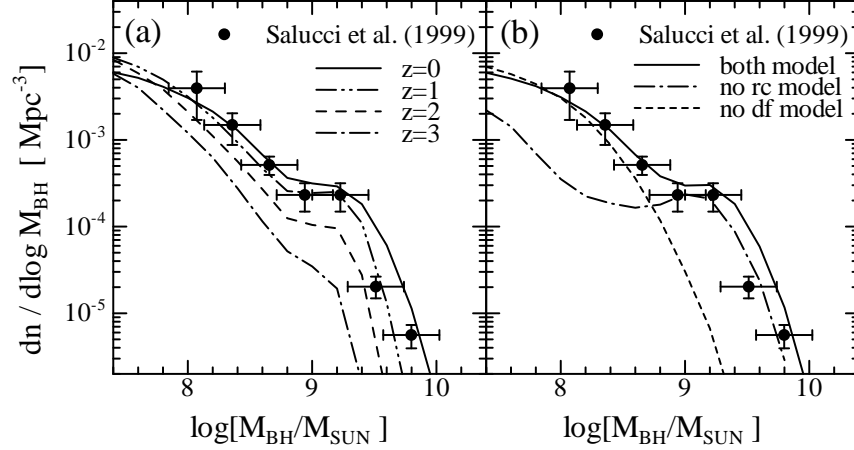


FIG. 2.— (a) Black hole mass function of the model at a series of redshifts. The solid, dot-dot-dashed, dashed and dot-dashed lines indicate the results at $z = 0, 1, 2$, and 3 , respectively. The symbols with errorbars are the present black hole mass function obtained by Salucci et al. (1999). (b) Black hole mass function of models for three models at $z = 0$. The solid, dot-dashed and short dashed lines indicate both model, no random collision model (no rc model) and no dynamical friction model (no df model), respectively. Both model includes dynamical friction and random collision as the galaxy merging mechanism.

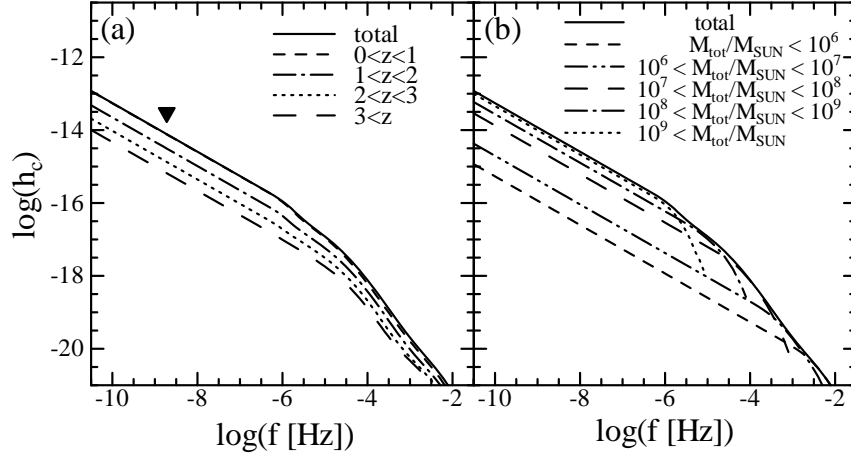


FIG. 3.— Spectrum of gravitational wave background radiation, $h_c(f)$, from SMBH binaries in different redshift intervals (a) and in different total mass ranges (b). (a) The total spectrum (solid line) and the other lines show those in different redshift intervals $0 \leq z < 1$ (dashed line), $1 \leq z < 2$ (dot-dashed), $2 \leq z < 3$ (short dashed) and $3 \leq z$ (long dashed). The filled reverse triangle shows the current limit from pulsar timing measurements Lommen (2002). (b) The total spectrum (solid line) and the other lines show those in different total mass intervals $M_{\text{tot}} \leq 10^6 M_\odot$ (dashed line), $10^6 M_\odot < M_{\text{tot}} \leq 10^7 M_\odot$ (dot-dot-dashed), $10^7 M_\odot < M_{\text{tot}} \leq 10^8 M_\odot$ (long dashed), $10^8 M_\odot < M_{\text{tot}} \leq 10^9 M_\odot$ (dot-dashed) and $10^9 M_\odot < M_{\text{tot}}$ (short dashed).

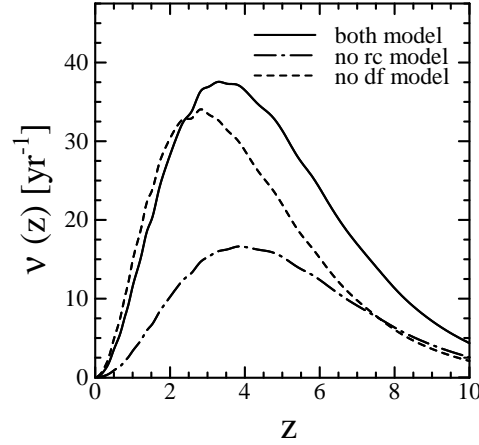


FIG. 4.— SMBH coalescence rate in observers' time unit a year, $\nu(z)$. The solid, dot-dashed and short dashed lines indicate both model, no random collision model (no rc model) and no dynamical friction model (no df model), respectively. Both model includes dynamical friction and random collision as the galaxy merging mechanism.

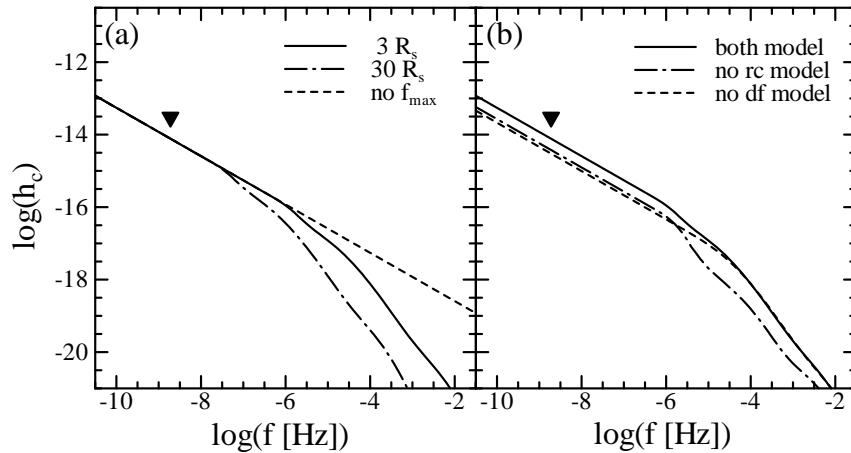


FIG. 5.— Spectrum of gravitational wave background radiation, $h_c(f)$, in different f_{max} (a) and in different galaxy merger models (b). The filled reverse triangle shows the current limit from pulsar timing measurements Lommen (2002). (a) The solid, dot-dashed and short dashed lines indicate the results with f_{max} corresponding to $3R_s$, $30R_s$ and no frequency cut off, respectively. (b) The solid, dot-dashed and short dashed lines indicate both, no random collision model (no rc model) and no dynamical friction model (no df model), respectively. Both model includes dynamical friction and random collision as the galaxy merging mechanism.

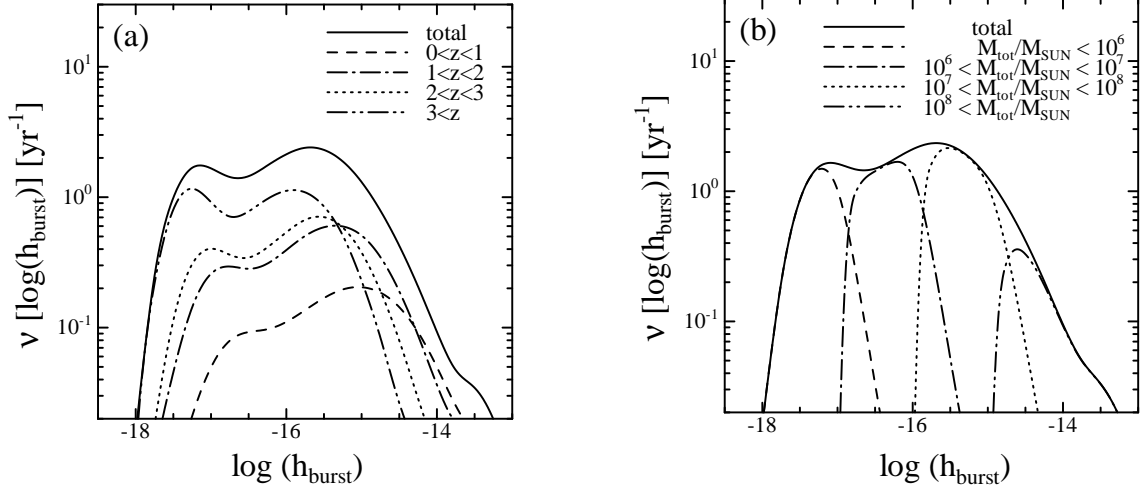


FIG. 6.— Integrated event rate of gravitational wave burst per observers' time unit a year $\nu_{\text{burst}}[\log(h_{\text{burst}})]$. (a) The total integrated event rate (solid line) and the other lines show those in different redshift intervals $0 \leq z < 1$ (dot), $1 \leq z < 2$ (dot-dashed), $2 \leq z < 3$ (short dashed) and $3 \leq z$ (dot-dot-dashed). (b) The total integrated event rate (solid line) and the other lines show those in different black hole mass intervals $M_{\text{tot}} \leq 10^6 M_{\odot}$ (dashed line), $10^6 M_{\odot} < M_{\text{tot}} \leq 10^7 M_{\odot}$ (dot-dashed), $10^7 M_{\odot} < M_{\text{tot}} \leq 10^8 M_{\odot}$ (dot) and $10^8 M_{\odot} < M_{\text{tot}}$ (dot-dot-dashed).

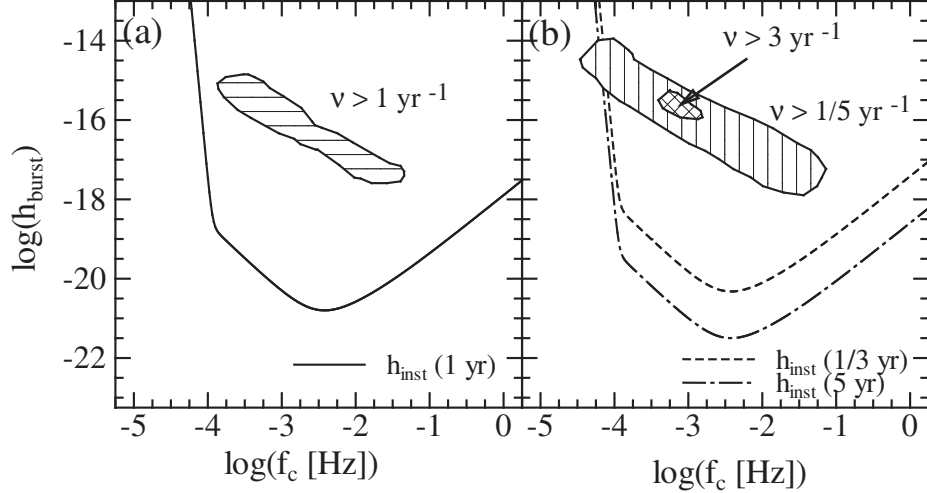


FIG. 7.— Expected signals of gravitational burst from SMBH. (a) The horizontally hatched area shows the region, $\nu_{\text{burst}}[\log(h_{\text{burst}}), \log(f_c)] > 1 \text{ yr}^{-1}$. The solid curve indicates the instrumental noise threshold for one year of LISA observations. (b) The vertically hatched area shows the region, $\nu_{\text{burst}}[\log(h_{\text{burst}}), \log(f_c)] > 1/5 \text{ yr}^{-1}$ and the diagonal cross-hatched area show the region, $\nu_{\text{burst}}[\log(h_{\text{burst}}), \log(f_c)] > 3 \text{ yr}^{-1}$. The dot-dashed and the short dashed lines indicates the instrumental noise threshold for 5 year and 1/3 year of LISA observations, respectively.